DOI: 10.13009/EUCASS2025-095
11TH EUROPEAN CONFERENCE FOR AERONAUTICS AND SPACE SCIENCES (EUCASS)

Comparative Electro-Aero-Dynamic propulsive properties of periodic and ducted electrode systems

Benoit Flesselles[1,2], *Franck Plouraboue*[1†] *and Nicolas Binder*[2]
[1]*Fluid Mechanics Institute of Toulouse (IMFT)*
Toulouse University, CNRS, INPT, UPS, 2 Allée du Pr. Camille Soula, 31400 Toulouse, France
[2]*Aerodynamic, Energetic & Propulsion Dept (DAEP)*
ISAE-SUPAERO, Université de Toulouse, 10 Ave Edouard Belin BP 54032, F-31055 Toulouse 4, France
benoit.flesselles@imft.fr · [†]fplourab@imft.fr · nicolas.binder@isae-supaero.fr
[†]Corresponding author

Abstract

The development of ducted multi-staged Electro-Aero-Dynamic (EAD) thrusters, as pioneered by Gómez-Vega et al.,[7,8] has demonstrated significant enhancement of thrust density compared with previous EAD thrusters. In this context, the present study investigates the confinement effects for the electrical and propulsive dynamics of a single-stage electrode configuration. This contribution is more precisely focused on the comparison between transversely periodic setups of electrodes (wire-to-cylinder thrusters) that have transverse spatial period Δ, and similar configurations confined between two parallel insulating dielectric walls separated by the same distance Δ. Experimental and numerical investigations both show an optimal distance $\Delta^\star$ which maximises the EAD thrust force for both confined and periodic configurations. Nevertheless, a 15-20% thrust increase is found in the case of both confined and periodic configurations as compared to unconfined aperiodic ones, showing the beneficial effect of appropriately positioned parallel insulating dielectric walls to mitigate the emitter's electrostatic shielding.

1. Introduction

1.1 Context

Electro-hydrodynamic (EHD) propulsion in air (EAD) has been considered for a long time,[3] although it has also been identified as inefficient. The main physical mechanisms leading to EAD thrust were soon identified as being the momentum transfer from accelerated ions drifting away from one electrode (referred to as the "emitter" in this context) into neutral air molecules. For a flying object moving at constant speed, imposing a stationary momentum transfer into air in its Lagrangian frame of reference, the total force balance between it and a controlled air volume leads to an effective EAD thrust, as for any propelling system. The charges responsible for EAD are generally created in thin regions where a high electric field generates a cold plasma. These thin regions depend on the chosen plasma's source, but in this contribution (as many others, e.g.[2,7,10,12,13,15,16,19,20]) the plasma source is a corona discharge.

The related poor propulsive efficiency[2,10,15,16,20] has restrained most research interests for aerodynamics applications for many years.[21] Nevertheless, recent advances have renewed its interest in specific contexts. First, Gilmore & Barrett[5,6] found that albeit poorly efficient whilst also very modest in thrust performances, EAD propulsion was on the contrary very good when considering its thrust-to-power ratio, from 10 to 20 N/kW, as compared to 2 N/kW for turbofan engines, and 10 N/kW for turboprop engines. Second, it has been recently demonstrated to be capable of a (short) autonomous flight on board a five-meter wingspan drone.[23] Third, it has been found capable to sustain the stationary flight of gliders, such as Solar Impulse II.[12] Fourth, it is a unique example of a solid-state propulsion system without moving parts, with the very specific advantage of being almost silent and environmentally friendly.

Recent advances have also demonstrated improved thrust density with thruster arrays[1,22] as well as multi-stage configurations.[19] Later, a ten-stage system of emitting/collecting electrodes coupled within an aerodynamic duct was found to produce an order of magnitude higher thrust density than a single stage array.[7] In the previous case, the duct is used for its aerodynamic properties ; however, introducing a dielectric duct close to the electrodes also modifies the electric field between the electrodes, due to surface charges depositing on the surface of the duct. This work focuses its analysis on quantifying the beneficial effect of electrostatically confined configurations compared with periodic ones. The term "confined" is employed to specifically denote the influence of electrostatic boundary conditions, whereas

DOI: 10.13009/EUCASS2025-095

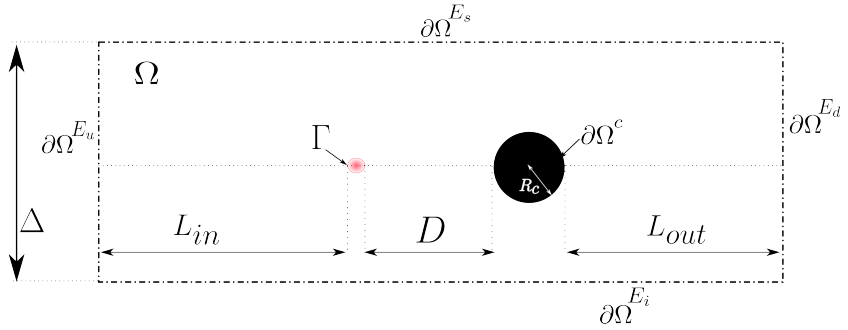

Figure 1: Geometry used for the numerical simulations where Ω is the air domain, excluding both the corona discharge (red spot having boundary Γ) and the cylindrical (black) collector having radius R_c. Apart from Γ, the Ω frontiers include the collector surface $\partial\Omega^c$ as well as external boundaries $\partial\Omega^E \equiv \partial\Omega^{E_u} \cup \partial\Omega^{E_s} \cup \partial\Omega^{E_d} \cup \partial\Omega^{E_i}$ (where index u, s, d, i stands for upstream, superior, downstream, inferior). Δ is the transverse distance between the dielectric upper and lower parallel planes.

in the literature "ducted" typically refers to modifications in fluid flow characteristics within an enclosed channel. As discussed in[6] and further investigated in,[9] periodic emitter configurations are submitted to electrostatic shielding, impinging their ability to ignite and leading to the inability of compact multiple emitters to improve thrust density. The question of whether ducted electrode systems compare with periodic ones is thus investigated in this contribution.

1.2 One-way coupling and drift-diffusion modelling

In the context of zero externally imposed velocity, the air flow resulting from EAD is referred to as ionic wind. Depending on the considered configuration and the electrode system, this velocity is generally of the order of a few meters per second, and can exceptionally rise to 16m/s in multi-stage systems.[19] This mostly results in a Reynolds number range of $10 - 10^3$, generally below the turbulent regime, but also into an electro-drift velocity that is much larger than the advective one. The electro-drift velocity is defined as $V_D = \mu E$, being the product between the ions' mobility $\mu[m^2/V.s]$ —V for Volt — and the local electric field $E[V.m^{-1}]$. Considering a value of ion mobility in air in atmospheric conditions $\mu = 2 \times 10^{-4}[m^2/V.s]$ (which is considered as the reference values up to 30%) and a reference electric field $E = 5 \times 10^5 V/m$ leads to a drift velocity $V_D \approx 100 m/s$, which is much larger than the induced ionic wind speed. This results in a simplified framework where EAD effects dominate over hydrodynamics, so that they act in only one direction, with the air being enslaved to the Coulomb forcing imposed by electrostatic forces. In this one-way coupling framework, the charges are submitted to electro-drift only, from negligible advection, so that the effective charge density ρ $[C/m^3]$ steady-state conservation reads:

$$\nabla \cdot (-\mu\rho\nabla\phi - D_\rho \nabla\rho) = 0, \tag{1}$$

with D_ρ $[m^2/s]$ the charge diffusivity, and ϕ $[V \cdot m]$ the electric potential verifying the electrostatic Maxwell-Gauss equation:

$$\Delta\phi = -\frac{\rho}{\epsilon_0}, \tag{2}$$

ϵ_0 being the dielectric permittivity of free space. Some boundary conditions are needed to complete (1) and (2). Denoting the V the electric potential applied between the electrodes, the following boundary conditions at surface Γ for emitter and surface $\partial\Omega^c$ for collector are considered:

$$\phi|_\Gamma = V \tag{3}$$

$$\phi|_{\partial\Omega^c} = 0. \tag{4}$$

For every other external boundaries $\partial\Omega^E \equiv \partial\Omega^{E_u} \cup \partial\Omega^{E_s} \cup \partial\Omega^{E_d} \cup \partial\Omega^{E_i}$ (where index u, s, d, i stands for upstream, superior, downstream, inferior; cf Figure 1) of boundary conditions zero electric field imposed and absence of charges leaks at lateral boundaries in the confined case:

$$\nabla\phi \cdot \mathbf{n}|_{\partial\Omega^E} = 0 \tag{5}$$

$$\nabla n \cdot \mathbf{n}|_{\partial\Omega^E} = 0 \tag{6}$$

DOI: 10.13009/EUCASS2025-095

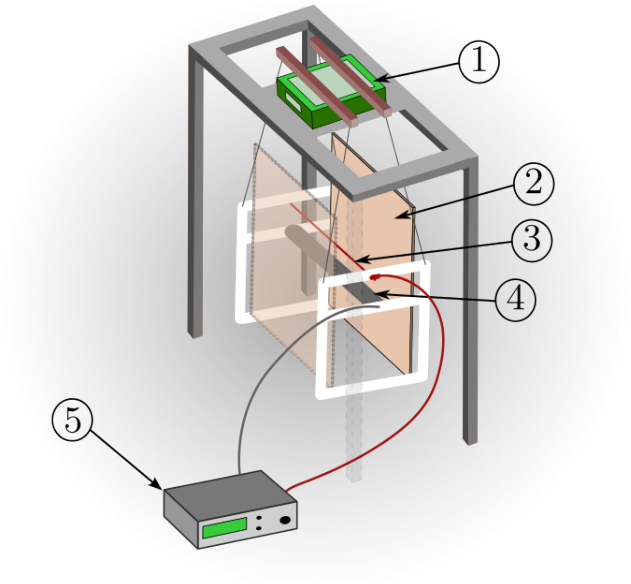

Figure 2: Experimental setup. ① Digital scale. ② Dielectric confinement plate. ③ Emitter electrode. ④ Collector electrode. ⑤ High-voltage power supply.

In the periodic case, only the borders $\partial\Omega^{E_s}$ and $\partial\Omega^{E_i}$ are treated differently: a periodicity condition is prescribed.

Last but not least, a further non-trivial boundary condition needs to be specified in the context where corona discharge modelling is discarded. Indeed, the multi-physics modelling of corona discharge is complex,[11] and not always useful in order to obtain relevant hydrodynamic modelling for ionic wind as shown in Picella et al.[18] Hence, in the following, the Kaptzov approximation is used, considering that an effective constant electric field applies at the emitter boundary Γ (Cf[14] for more details)

$$\nabla\phi \cdot \mathbf{n}|_\Gamma = E_a, \tag{7}$$

with E_a either given by Peek's formula[17] or some asymptotic approximation.[14] This drift-diffusion model is used to obtain current-voltage predictions for various electrode configurations exposed to confined or periodic boundary conditions.

1.3 Experimental setup

Figure 2 presents the experimental setup, which closely follows the configuration described by Monrolin et al.[12] The thrust generated by the system was measured by weighing the apparatus using a precision scale. The two dielectric walls were mounted within a PTFE frame suspended by nylon wires from a high-precision Sartorius BCE4202I-1S Entris II weighing scale, which has a resolution of 0.01 g, as depicted in Figure 2. To minimise parasitic electrostatic forces, the distance between the bottom of the dielectric confinement plates and the ground was maintained at a minimum of 60 cm, and the top of the plates was kept at least 60 cm away from the wooden structure supporting the scale. Furthermore, the PTFE frame was positioned at least 2 m away from the room's walls.

The weighing scale rests on a 2 cm-thick wooden plate to ensure stability, supported by a wooden structure. The total mass of the suspended assembly, including the emitter, cylindrical collector, and wiring, was measured as 2133 g without the dielectric plates and 3418 g with the dielectric plates installed. The scale's maximum nominal load was 4200 g. Two high-voltage power supplies (Iseg HP700505p and Iseg HP700505n) were employed to provide positive and negative voltages, respectively, up to 70 kV. These power supplies were used sequentially during the experiments, as detailed in the following section. The high-voltage lead consisted of a shielded, rigid cable; however, to minimise any influence on the weight measurements, the connection between the high-voltage lead and the emitter copper tip has been done using a flexible, insulated copper multistrand wire with a cross-sectional area of 1 mm^2. Two parallel electrodes were positioned symmetrically within the mid-plane between two planar, parallel dielectric walls, each with a thickness of $t_w = 5$ mm, a span of $L_s = 390$ mm, and a length of $L = 690$ mm, as illustrated in Figure 2. To prevent the accumulation of electrostatic charges on the outer surfaces, both external faces of the dielectric walls were covered with grounded metallic sheets. This assembly was secured within a PTFE frame, suspended from the scale using nylon line. This configuration was deliberately chosen to isolate electrostatic effects attributable to 2D spatial confinement. Notably, this setup does not constitute a fully ducted configuration, as dielectric plates were not installed at the electrode

DOI: 10.13009/EUCASS2025-095

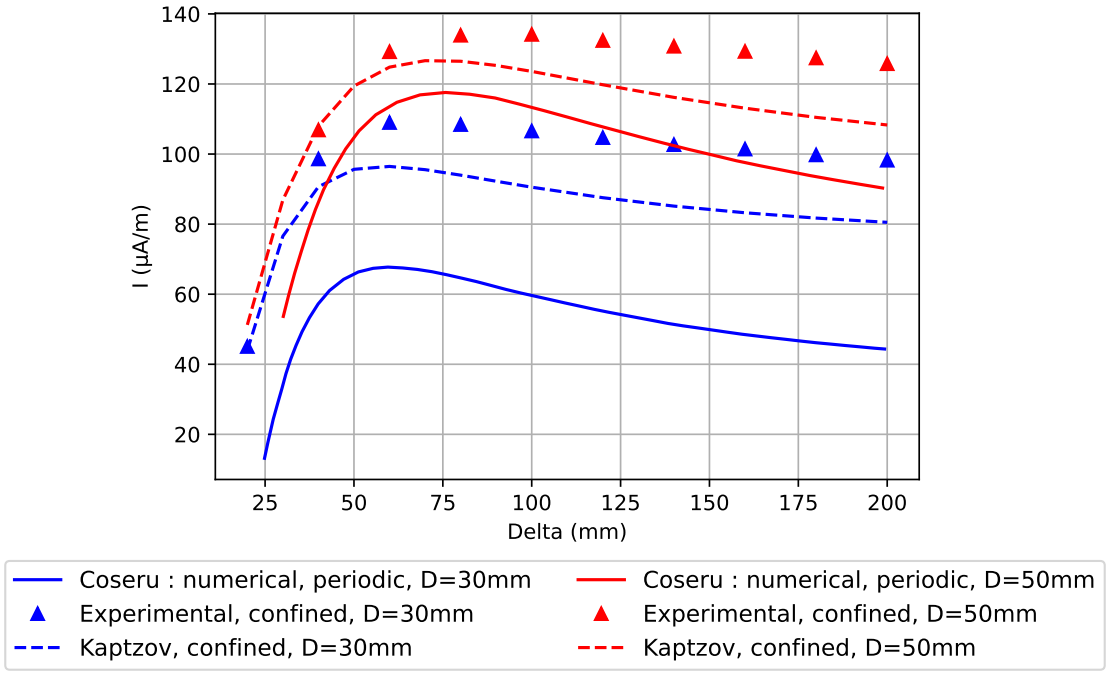

Figure 3: Experimental and numerical current intensity I.

extremities, hence the use of the term "confined". The emitter consisted of a copper wire with a diameter of $d_e = 75\mu$m, with both extremities welded onto small copper tips mounted on either side of the PTFE frame (see Figure 2).

2. Results

Figure 3 compares the electrical current I obtained by Coseru et al.[4] from numerical simulation in periodic thrusters of periodicity Δ, with numerical and experimental current values obtained in confined configurations with inter-wall distance Δ, for two emitter-collector face-to-face distances $D = 30$mm and $D = 50$mm, and various distances Δ. In every case, the applied voltage was chosen such that the mean electric field was kept at a constant value $E = V/D = 4.5$kV. Although all curves exhibit a similar trend, significant quantitative differences are observed between the numerical periodic current values, numerical confined current values, and experimental confined current values, the origin of which is discussed in the following section. However, the observed similar trend is noteworthy: in every case, the current strongly increases for lower values of Δ, reaching a maximum for a clear given value $\Delta^\star$, then decreases towards an asymptotic value for higher values of Δ. In both confined and periodic configurations, the values of $\Delta^\star$ maximising the current are very similar, approximately equal to $\Delta^\star = 60$ mm for $D = 30$ mm and $\Delta^\star = 75$ mm for $D = 50$ mm, which is very close to the experimental measurement. For $D = 50$ mm, the increase in current in comparison with the plain emitter-collector pair is less important in the experimental measurements than in the numerical configurations. It seems to appear for higher values of $\Delta \approx 90$ mm. It is unclear whether this difference could be attributable to experimental bias or numerical modelling issues.

Figure 4 shows EAD thrust F obtained in the same configurations as described above. Similarly to the current curves, there exists an optimal $\Delta^\star$ value maximising thrust. It thus decreases sharply as Δ approaches zero, and tends to an asymptotic value as Δ approaches infinity. This trend is not surprising, given that EAD thrust is usually considered proportional to current: $F = ID/\mu$, with μ the ionic mobility.[12] However, it is noteworthy that the thrust obtained in confined simulations is almost equal to that obtained in corresponding periodic simulations, while current values differ significantly in the same configurations. The large difference between experimental and numerical simulation results is mainly due to omitting the collector drag in the latter since no hydrodynamic effects have been taken into account in the modelling. However, the observed difference between the predicted pure EAD thrust and the experimental observed one, is very close with the one observed in Coseru et al.[4] Estimating this difference as the drag correction given in the same article[4] leads to an overestimation of about 5 mN for the $D = 50$ mm case and 3 mN for the $D = 50$ mm case, which is close to the observed discrepancy. Given that numerical simulations in periodic and confined configurations show a very similar thrust, but distinct currents, the thrust-to-power ratio is expected to be

DOI: 10.13009/EUCASS2025-095

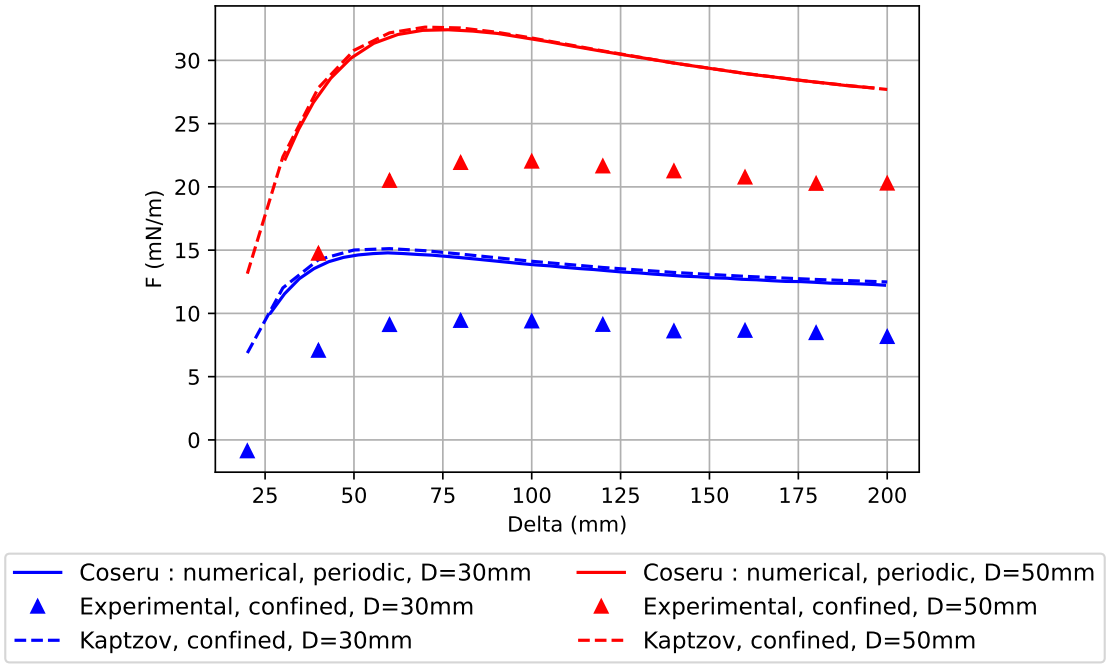

Figure 4: Experimental and numerical thrust F.

lower in the confined case. This is especially true in the $D = 30$ mm case, where $I_{confined}(\Delta^\star)/I_{periodic}(\Delta^\star) = 1.42$. Given that both cases use identical voltage and produce identical thrust, leads to a thrust to power $\Theta = F/(IV)$ relative increase of approximately 40% at $\Delta^\star$ for the periodic configuration compared to the confined configuration. This effect is weaker in the $D = 50$ mm case, where thrust-to-power in the periodic case is 8% higher in the periodic case than in the confined case. It is unclear why the confined case would produce more current but identical thrust in the described configurations.

3. Discussion

As explained in section 1.2, confined and periodic configurations appear very similar from the numerical point of view, which is confirmed by the similar results obtained in both numerical studies. Experimental results in a corresponding confined configuration are in good agreement with numerical simulations. However, the present work did not consider experimental periodic configurations for comparison. Periodic configurations are indeed difficult to build experimentally,[1] while at the same time also difficult to reliably compare with a strictly periodic array. As discussed in Lemetayer et al.,[9] the external emitters of a finite-size array display a distinct ignition threshold. Depending on the emitter-collector distance, external emitters can even ignite beforehand, and subsequently shield the ignition of the inner emitters (Cf Lemetayer et al.[9] for further details). Hence, experiments face unavoidable finite-size effects when trying to map periodic configurations, some of them detrimental to direct comparison. In addition, the physical alignment of each emitter line in the array is another source of possible experimental issue. These are serious reasons for tempering the absence of experimental investigation in periodic configurations. Furthermore, some quantitative discrepancies remain between the numerical and experimental data presented above in ducted configurations.

A potential source of discrepancy is the slight difference in emitter radius between the periodic numerical simulations carried out by Coseru et al.[4] and the confined experiments and simulations presented in this work. Coseru et al.[4] have considered an emitter diameter $r_{em} = 79.90\mu$m, whereas an emitter diameter of 75μm is used in the present investigation, both in numerical and experimental sections. Figure 6 compares the intensity I computed in a confined configuration for both emitter radii where one can observe that the relative error predicted when changing the emitter radii is under 2% in the worst case.

Another potential source of discrepancy could be the use of Peek's empirical formula (8) for the critical onset field E_a used in boundary condition (7)

$$E_a = 3 \times 10^6 \left(1 + \frac{0.0301}{\sqrt{r_{em}}}\right) \tag{8}$$

DOI: 10.13009/EUCASS2025-095

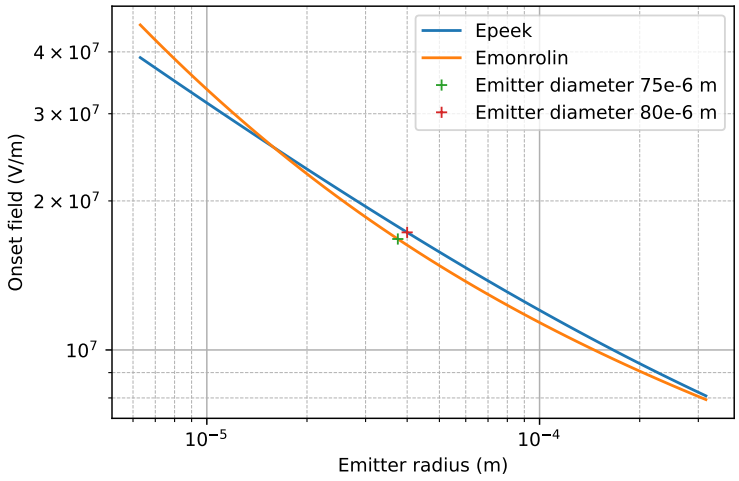

Figure 5: Variation in critical field E_a calculated with Peek's[17] and Monrolin et al.[14] formula.

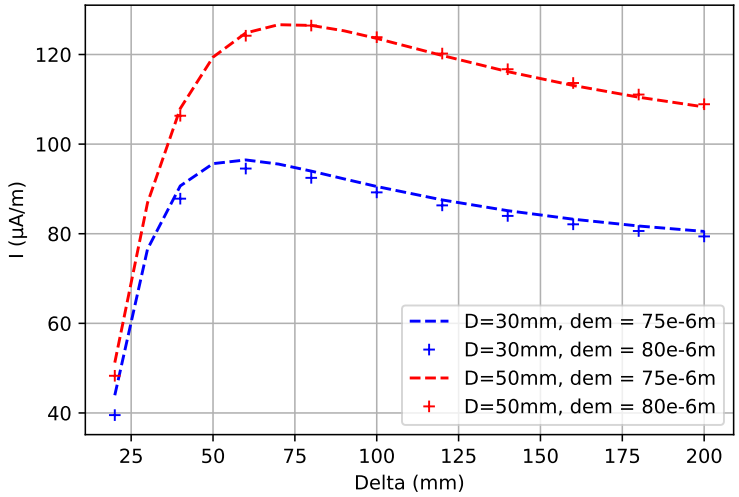

Figure 6: Experimental measurement of the electrical current I for two emitter radii, and two emitter-collector distances D.

Monrolin et al.[14] proposed an alternative asymptotic derivation allowing a more precise calculation of E_a

$$E_a = E_i \mathcal{W}_0 \left(\frac{r_{em}\beta}{\ln(1+\gamma^{-1})} \right)^{-1}, \tag{9}$$

where β and E_i are physical parameters involved in computing Townsend's first ionisation coefficient $\alpha = \beta \exp(-E_i/E)$, and γ is a photoionisation coefficient. Values used in the present work were taken from Monrolin et al.:[14] $E_i = 2.09 \times 10^7 \mathrm{V/m}$, $\beta = 7.2 \times 10^5 \mathrm{m}^{-1}$, and $\gamma = 2 \times 10^{-3}$.

Figure 5 compares critical ignition values obtained with either (8) or (9) imposed electric field at boundary Γ, for a wide range of emitter diameters. For the emitter diameters considered in this work, using Peek's law rather than Monrolin et al.'s formula results in a slight overestimation of the critical onset field, which in turn leads to similar overestimation of the onset voltage. As a result, the thrust and current in Coseru et al.[4] simulations may be slightly underestimated.

Furthermore, the influence of the stream-wise length of the simulation domain has been explored by varying the lengths L_{in} and L_{out} defined in Figure 1. Figure 7 shows the resulting relative error for the computed electrical current for two configurations: $L_{in} = L_{out} = 15\mathrm{cm}$ and $L_{in} = L_{out} = 40\mathrm{cm}$. It can be seen that although the error increases for larger values of Δ, it remains under 0.03%, which is significantly lower than the previously considered errors.

DOI: 10.13009/EUCASS2025-095

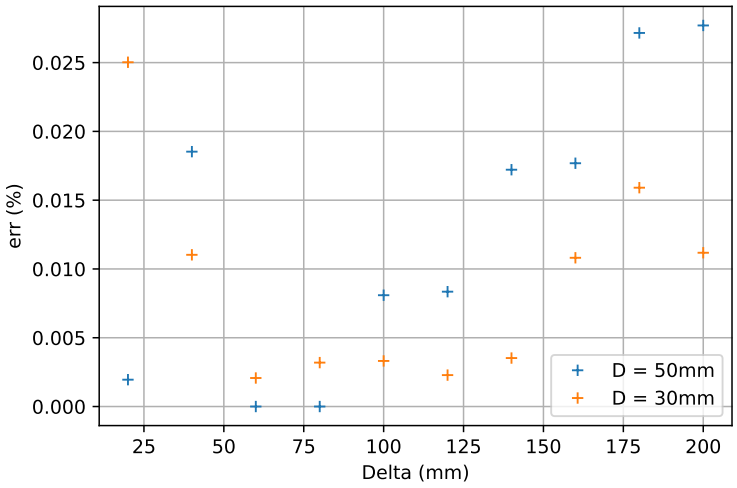

Figure 7: Relative error in simulated current I for two domain lengths.

4. Conclusion

This study has systematically investigated the propulsive and electrical performance of single-stage Electro-Aero-Dynamic (EAD) thrusters under both transversely periodic and duct-confined configurations. Experimental and numerical results demonstrate that spatial confinement, achieved either through periodic electrode arrays or dielectric walls separated by an optimal distance $\Delta^\star$, leads to an increase in thrust force of 15-20% compared to unconfined single-stage single thruster systems. The shared optimal spacing $\Delta^\star$ between periodic and confined configurations suggests a universal mechanism for mitigating electrostatic shielding while enforcing streamwise flow. However, the recorded differences in current prediction are not yet fully understood and require experimental validation. Regarding force generation, no significant variation is expected, according to the simulation results. However, the discrepancies in current suggest an equivalent influence on the efficiency of the thruster, which should be further investigated.

These findings provide clear evidence that transverse confinement, whether realised through periodic placement or dielectric walls, is a critical factor in maximising EAD thrust density. This equivalence between periodic and confined setups provides valuable flexibility for designing compact, high-efficiency EAD thrusters. Future work should further explore the scalability of these principles to multi-stage and fully ducted configurations.

5. Acknowledgments

This project has received a co-funding from CNES-DGA Allocation doctorale CONVENTION N^o 240777/00.

References

[1] Marco Belan, Raffaello Terenzi, Stefano Trovato, and Davide Usuelli. Effects of the emitters density on the performance of an atmospheric ionic thruster. *Journal of Electrostatics*, 120:103767, November 2022.

[2] E.A. Christenson and P.S. Moller. Ion-Neutral Propulsion in Atmospheric Media. *AIAA. J.*, 5(10):1768–1773, 1967.

[3] Edward A. Christenson and Paul S. Moller. Ion-neutral propulsion in atmospheric media. *AIAA Journal*, 5(10):1768–1773, October 1967.

[4] Christian Coseru, David Fabre, and Franck Plouraboué. Numerical study of ElectroAeroDynamic force and current resulting from ionic wind in emitter/collector systems. *Journal of Applied Physics*, 129(10):103304, March 2021. Publisher: American Institute of Physics.

[5] Christopher K. Gilmore and S. R. H. Barrett. Electrohydrodynamic thrust density using positive corona-induced ionic winds for in-atmosphere propulsion. *Proc. R. Soc. A*, 471(2175):20140912–20140912, 2015.

DOI: 10.13009/EUCASS2025-095

[6] Christopher K Gilmore and Steven R H Barrett. Electroaerodynamic thruster performance as a function of altitude and flight speed. *AIAA. J.*, 56(3):1105–1117, 2017.

[7] Nicolas Gomez-Vega and Steven R. H. Barrett. Order-of-Magnitude Improvement in Electroaerodynamic Thrust Density with Multistaged Ducted Thrusters. *AIAA Journal*, 62(4):1342–1353, April 2024.

[8] Nicolas Gomez-Vega, Arthur Brown, Haofeng Xu, and Steven R. H. Barrett. Model of Multistaged Ducted Thrusters for High-Thrust-Density Electroaerodynamic Propulsion. *AIAA Journal*, 61(2):767–779, February 2023.

[9] Julien Lemetayer, Corentin Marion, David Fabre, and Franck Plouraboué. Multi-inception patterns of emitter array/collector systems in DC corona discharge. *Journal of Physics D: Applied Physics*, 55(18):185203, 2022. Publisher: IOP Publishing.

[10] Kento Masuyama and S. R. H. Barrett. On the Performance of electrohydrodynamic propulsion. *Proc. R. Soc. A*, 50(6):1480–1486, 2013.

[11] Nicolas Monrolin and Franck Plouraboué. Multi-scale two-domain numerical modeling of stationary positive DC corona discharge/drift-region coupling. *Journal of Computational Physics*, 443:110517, October 2021.

[12] Nicolas Monrolin, Franck Plouraboué, and Olivier Praud. Electrohydrodynamic Thrust for In-Atmosphere Propulsion. *AIAA. J.*, 55(12):4296–4305, 2017.

[13] Nicolas Monrolin, Olivier Praud, and Franck Plouraboué. Electrohydrodynamic ionic wind, force field, and ionic mobility in a positive dc wire-to-cylinders corona discharge in air. *Phys. Rev. Fluids*, 3(6):063701, 2018.

[14] Nicolas Monrolin, Olivier Praud, and Franck Plouraboué. Revisiting the positive DC corona discharge theory: Beyond Peek's and Townsend's law. *Phys. Plasmas*, 25:063503, 2018.

[15] Eric Moreau, Nicolas Benard, Jean-Daniel Lan-Sun-Luk, and Jean-Pierre Chabriat. Electrohydrodynamic force produced by a wire-to-cylinder dc corona discharge in air at atmospheric pressure. *Journal of Physics D: Applied Physics*, 46(47):475204, November 2013.

[16] Eric Moreau and Gérard Touchard. Enhancing the mechanical efficiency of electric wind in corona discharges. *J. Electrostat.*, 66(1-2):39–44, 2008.

[17] Franck William Peek. *Dielectric phenomena in high voltage engineering*. McGrow-Hill Book Company, New-York, 1915.

[18] F. Picella, D. Fabre, and F. Plouraboué. Numerical simulations of ionic wind induced by positive DC-corona discharges. *AIAA. J.*, 62(7):2562–2573, 2024.

[19] W. Qiu, L. Xia, L. Yang, Q. Zhang, L. Xiao, and L. Chen. Experimental study on the velocity and efficiency characteristics of a serial staged needle array-mesh type ehd gas pump. *Plasma Science and Technology*, 13(6):693–697, 2011.

[20] Myron Robinson. Movement of air in the electric wind of the corona discharge. *T. Am. Inst. Elect. Eng.*, 80(2):143–150, 1961.

[21] Jack Wilson, Hugh Perkins, and William Thompson. An investigation of ionic wind propulsion. Technical report, NASA Report NASA/TM, 2009.

[22] Jack Wilson, Hugh D Perkins, and William K Thompson. An Investigation of Ionic Wind Propulsion. 2009.

[23] Haofeng Xu, Yiou He, Kieran L. Strobel, Christopher K. Gilmore, Sean P. Kelley, Cooper C. Hennick, Thomas Sebastian, Mark R. Woolston, David J. Perreault, and Steven R. H. Barrett. Flight of an aeroplane with solid-state propulsion. *Nature*, 563(7732):532+, 2018.